HHS Public Access

Author manuscript

Cell. Author manuscript; available in PMC 2018 January 26.

Published in final edited form as:

Cell. 2017 January 26; 168(3): 413–426.e12. doi:10.1016/j.cell.2017.01.005.

Cellular and Circuit Mechanisms Shaping the Perceptual Properties of the Primate Fovea

Raunak Sinha[1,2,*], **Mrinalini Hoon**[3,*], **Jacob Baudin**[1,2], **Haruhisa Okawa**[3], **Rachel O.L. Wong**[3], and **Fred Rieke**[1,2,4,*]

[1]Department of Physiology and Biophysics, University of Washington, Seattle, Washington 98195, USA

[2]Howard Hughes Medical Institute. University of Washington, Seattle, Washington 98195, USA

[3]Department of Biological Structure, University of Washington, Seattle, Washington 98195, USA

SUMMARY

The fovea is a specialized region of the retina that dominates the visual perception of primates by providing high chromatic and spatial acuity. While the foveal and peripheral retina share a similar core circuit architecture, they exhibit profound functional differences whose mechanisms are unknown. Using intracellular recordings and structure-function analyses, we examined the cellular and synaptic underpinnings of the primate fovea. Compared to peripheral vision, the fovea displays decreased sensitivity to rapid variations in light inputs; this difference is reflected in the responses of ganglion cells, the output cells of the retina. Surprisingly, and unlike in the periphery, synaptic inhibition minimally shaped the responses of foveal midget ganglion cells. This difference in inhibition cannot however, explain the differences in the temporal sensitivity of foveal and peripheral midget ganglion cells. Instead, foveal cone photoreceptors themselves exhibit slower light responses than peripheral cones, unexpectedly linking cone signals to perceptual sensitivity.

Graphical abstract

[*]Correspondence: rsinha@uw.edu (R.S.), mhoon@uw.edu (M.H.), rieke@uw.edu (F.R.).
[4]Lead Contact

SUPPLEMENTAL INFORMATION

Supplemental Information contains seven figures and can be found with this article online at http://dx.doi.org/10.1016/j.cell.2017.01.005.

AUTHOR CONTRIBUTIONS

R.S., F.R. and J.B. performed the electrophysiological recordings and analysis. M.H. performed the immunohistochemistry, biolistics and all the anatomical analysis. H.O. helped with the biolistic experiments and image analysis. R.S., M.H. and F.R. conceived of experiments and analyses. R.S., M.H., R.O.W. and F.R. wrote the paper.

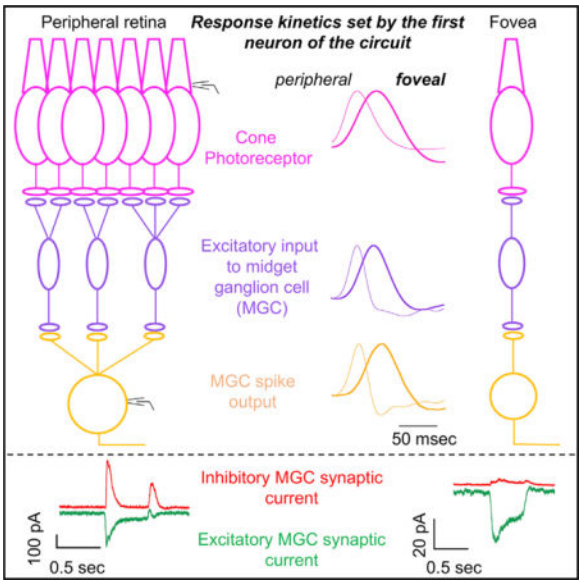

INTRODUCTION

The fovea accounts for <1% of the surface area of the primate retina but accounts for ~50% of the retinal output neurons and provides input to ~50% of the cells in primary visual cortex (Wässle et al., 1989). Signals originating in the fovea enable the high chromatic and spatial acuity that dominate our everyday visual experience—including your ability to read this page. But foveal signaling limits sensitivity to other important aspects of the visual world. Specifically, perceptual sensitivity to rapidly-varying light inputs is lower for foveal vision than peripheral vision (Hecht and Verrijp, 1933), and this difference is present in the retinal outputs (Solomon et al., 2002). The low temporal sensitivity of foveal vision is reflected in the refresh rates of computer monitors and movies and will be an important factor in the design of visual prosthetics. The absence of a fovea in most mammals and technical challenges associated with intracellular recordings from the primate fovea mean that we know little about the cellular and synaptic basis of the functional differences between the fovea and peripheral retina.

The foveal and peripheral retina share a similar core circuit architecture: photoreceptors convey information to excitatory bipolar neurons that then convey information to output ganglion cells (Hoon et al., 2014). Inhibitory interneurons can modulate this core excitatory pathway. Given this common circuit architecture, differences in the temporal sensitivity of foveal and peripheral retinal outputs could originate in the cone photoreceptors themselves or in the neural circuits that read out the cone signals. A likely circuit mechanism is synaptic inhibition, which shapes kinetics of signals in many neural circuits (reviewed by Isaacson and Scanziani, 2011), including the retina (reviewed by Jadzinsky and Baccus, 2013). Inhibition can speed or slow responses depending on where it operates and how it interacts with other synaptic properties such as depression (Asari and Meister, 2012). The potential role of inhibition in shaping response kinetics is one example of a broader emergent theme in retinal research showing the importance of inner retinal inhibitory circuits in unexpected

and sophisticated computations (reviewed by Jadzinsky and Baccus, 2013) such as direction selectivity (Wei et al., 2011; Yonehara et al., 2011) and sensitivity to local but not global motion (Baccus et al., 2008). These computations are distinct from the outer retinal horizontal cell-mediated surround inhibition that shapes ganglion cell spatial receptive fields across the retina (Crook et al., 2011; McMahon et al., 2004; Wu, 1992).

Differences in temporal sensitivity could also originate in the cone photoreceptor responses. The importance of the kinetics of photoreceptor inputs to the retina is not without precedent: striking differences in the kinetics of the responses of rod and cone photoreceptors (Schneeweis and Schnapf, 1995) clearly contribute to night versus day differences in the temporal sensitivity of visual perception (Hecht and Verrijp, 1933). Cones themselves are often assumed functionally homogeneous across the retina except for differences in wavelength sensitivity, but this assumption has not been tested.

RESULTS

The results are organized around three main findings about the origin of differences in temporal sensitivity between foveal and peripheral midget ganglion cells (MGCs): (1) the kinetics of responses of foveal MGCs, unlike peripheral MGCs, are minimally shaped by synaptic inhibition; (2) consistent with this functional difference, foveal MGCs express fewer inhibitory postsynaptic receptors than their peripheral counterparts; and, (3) the kinetics of the responses of foveal and peripheral cones differ dramatically.

Midget Ganglion Cells Show Slower Response Kinetics in the Fovea than in the Periphery

In vivo recordings of responses to sinusoidal gratings show that responses of foveal MGCs decline more quickly with temporal frequency than those of peripheral MGCs (Solomon et al., 2002). To confirm that these differences are present in a preparation that allows access to the underlying cellular and synaptic mechanisms, we recorded spike responses in whole mount retina in an in vitro preparation. We compared MGC spike output in foveal (1 cone/MGC, 0–1 mm eccentricity, 0–4 degrees of visual angle, Figure 1A left), central (3–4 cones/MGC, 2–4 mm eccentricity, 8–16 degrees of visual angle, Figure 1A middle) and peripheral retina (10–20 cones/MGC, >6 mm eccentricity, (>24 degrees of visual angle, Figure 1A right). These regions differ dramatically in retinal circuitry and in the visual behavior that they support; notably foveal MGCs receive (indirectly via a midget bipolar cell) input from a single cone photoreceptor, forming a “private line” of signaling and the basis for the high spatial acuity of foveal vision, while central and peripheral MGCs receive (indirect) input from ~2–6 cones and ~10–30 cones, respectively (Calkins et al., 1994; Kolb and Marshak, 2003; Merigan et al., 1991; Schiller et al., 1990).

Full-field contrast steps elicited a robust increment in spike responses at the onset of the stimulus in ON MGCs—i.e., MGCs that depolarize to increases in light intensity (Figure 1B). The spike responses of peripheral MGCs to 100% contrast steps had a more pronounced transient peak compared to responses of foveal MGCs (Figure 1B). To further characterize MGC response kinetics, we presented a time-varying random stimulus and computed the average stimulus preceding a spike (the spike-triggered average or STA; Figures 1C–1E). The STA kinetics differed substantially, with foveal MGCs exhibiting the

slowest kinetics and peripheral MGCs exhibiting the fastest kinetics (Figures 1C and 1D). Kinetics of central MGCs fell between those of foveal and peripheral MGCs, indicating a smooth dependence of response kinetics on retinal eccentricity (Figures 1C and 1D).

Foveal MGCs Receive Little or No Light-Driven Inhibitory Synaptic Input

The gradient in kinetics of MGC spike output could be created upstream of the MGC in the retinal circuitry or by integration of excitatory and inhibitory synaptic inputs in the MGC. The balance of inhibitory and excitatory synapses (the I/E balance) shapes synaptic integration and signaling in many neural circuits (reviewed by Isaacson and Scanziani, 2011). This general importance of I/E balance underscores the importance of comparing MGC inhibitory and excitatory synaptic inputs across retinal locations (fovea, central and peripheral).

Full-field contrast steps elicited robust excitatory synaptic inputs to ON MGCs across retinal locations (Figure 2A). Excitatory synaptic inputs, like spike outputs, were more transient in peripheral MGCs compared to foveal and central MGCs (Figure 2A). Furthermore, MGC inhibitory synaptic inputs elicited by these (and other) stimuli varied dramatically across retinal regions, with the smallest inhibitory inputs in the fovea and largest in the periphery (Figures 2A, 2C–2F). OFF MGCs in the fovea also exhibited robust light-driven excitatory inputs and minimal inhibitory inputs (Figure 2B). Previous work in central retina (2–4 mm eccentricity) found, similarly, that drifting gratings elicit small inhibitory inputs to MGCs (Crook et al., 2011). The ratio of inhibitory to excitatory synaptic input (the I/E ratio) changed more than 10-fold between foveal and peripheral cells (Figures 2C and 2D).

Uncaging GABA and glutamate provided a further test of the generality of these results. GABA elicited a much smaller response relative to glutamate in foveal MGCs compared to peripheral MGCs (Figure 2G; see STAR Methods). The lack of light-driven inhibitory input was not an artifact of our recordings, as foveal MGCs received spontaneous inhibitory input that was not correlated with the onset of the light stimulus (Figure 2G).

Non-midget Ganglion Cells in the Fovea Exhibit Robust Postsynaptic Inhibition

Do other ganglion cells in the fovea share the near-complete lack of light-driven synaptic inhibition exhibited by MGCs? MGCs account for ~90% of the ganglion cells in the fovea; the remaining ~10% are ganglion cell types with wider dendritic fields, which correspondingly receive (indirect) input from multiple cones (Calkins and Sterling, 2007; Grünert et al., 1993). Non-MGC foveal cells are difficult to target for recording due to their sparsity and the similarity of their soma morphology to that of the much more numerous MGCs. Hence, we have compared the wide-field cells collectively to the MGCs. Figures 3A–3C shows examples of excitatory and inhibitory synaptic inputs to three foveal wide-field cells, and Figure 3D collects I/E ratios for foveal MGCs, foveal wide-field cells and peripheral MGCs. Among these cell types the foveal MGCs are unique in receiving minimal light-driven inhibitory synaptic input.

Foveal MGCs Express Low Levels of Inhibitory Postsynaptic Receptors Relative to Excitatory Postsynaptic Receptors

The lack of light-driven inhibitory input to foveal MGCs was surprising given the importance of inhibition in other neural circuits (reviewed by Isaacson and Scanziani, 2011) and the high density of presumed inhibitory (non-ribbon) synapses made onto foveal MGC dendrites as revealed by electron microscopy (Calkins et al., 1994; Calkins and Sterling, 1996; Kolb and Dekorver, 1991). These findings could be reconciled if the stimuli used in our physiological recordings failed to engage inhibitory circuits. Alternatively, postsynaptic expression of excitatory and inhibitory receptors could differ independent of synapse number. As described below, assessment of receptor expression in MGC dendrites across eccentricity supports the latter explanation.

Excitatory and inhibitory postsynaptic receptors on the dendrites of individual GCs were visualized by biolistic transfection with plasmids encoding several fluorescently labeled synaptic proteins: (1) postsynaptic density protein-95 (PSD95-CFP), a scaffolding protein at most retinal excitatory synapses (Koulen et al., 1998) and a “marker” for ionotropic glutamate receptors in retinal ganglion cells (Kerschensteiner et al., 2009; Morgan et al., 2008); (2) $GABA_A$ receptor subunits (α1-YFP, β2/3 and γ2); and, (3) tdTomato to visualize dendrites (Figures 4A and 4B). We labeled the $GABA_A$ α1 subunit because it is predominantly localized on primate MGCs (Abbott et al., 2012; Grünert et al., 1993). Fluorescently-tagged postsynaptic proteins were localized appropriately at their respective synapses (Figure S1).

To quantify expression of excitatory and inhibitory receptors, we estimated the percent of the dendritic volume occupied by PSD95-CFP and by $GABA_A\alpha$1-YFP (volume occupancy, see STAR Methods). Two results emerged. First, the ratio of $GABA_A$-YFP and PSD95-CFP expression (I/E ratio) was much smaller in foveal compared to peripheral MGCs (Figures 4B and 4D), consistent with the physiological observations. Second, wide-field ganglion cells in the fovea, such as parasol cells, exhibited considerably greater expression of inhibitory $GABA_A$-YFP receptors than nearby foveal MGCs, with a $GABA_A$-YFP/PSD95-CFP ratio near 1.0 (Figure 4D), also consistent with physiology (Figure 3).

Immunolabeling experiments provided additional evidence for the low expression of inhibitory receptors by foveal MGCs. Individual MGCs were filled with neurobiotin during physiological recordings and the retina was then immunostained with antibodies against the GluA3 subunit of the AMPA receptor (Figure 4C, raw images of immunostaining in Figure S2A) and gephyrin (Abbott et al., 2012; Fischer et al., 2000) or the α1 subunit of $GABA_A$ receptors (Grünert et al., 1993). We measured I/E ratios for individual cells by estimating volume occupancy of the synaptic markers (Figure S3). Foveal MGC dendrites exhibited low volume occupancy for endogenous gephyrin and $GABA_A\alpha$1 compared to GluA3 (i.e., low I/E ratio; Figure 4E), consistent with the biolistic results (Figure 4D) and the physiological recordings (Figure 2, Figure S2B). Further, peripheral MGC dendrites exhibited a near equal ratio of inhibitory and excitatory postsynaptic receptors (Figures 4C and 4E), as previously shown (Abbott et al., 2012) and consistent with our physiological measurements (Figure 2). Wide-field ganglion cells in the fovea displayed high $GABA_A\alpha$1 levels relative to MGCs (Figure S4).

Together, both biolistic and immunolabeling experiments show that foveal MGCs express relatively few inhibitory receptors, and that foveal and peripheral wide-field GCs that receive input from multiple cones express a much higher ratio of inhibitory to excitatory receptors. We compare these findings with electron microscopic measures of presynaptic structures in the Discussion.

Inhibitory Synaptic Input Regulates the Gain but Not Kinetics of the Peripheral MGC Spike Output

Does the strong gradient in the ratio of inhibitory to excitatory synaptic input received by MGCs across retinal locations account for the difference in MGC response kinetics? We used the dynamic clamp technique to determine how integration of excitatory and inhibitory inputs shapes the MGC spike output. These experiments measure the voltage changes elicited by injecting currents corresponding to light-evoked conductances. We used three sets of conductances measured in response to randomly-varying stimuli (Figure 5A): (1) the excitatory conductance measured from a foveal MGC; (2) excitatory and inhibitory conductances measured simultaneously (Cafaro and Rieke, 2010) from a peripheral MGC; and (3) the peripheral MGC excitatory conductance alone. Three conclusions emerged from comparing the spike responses and STAs of foveal and peripheral MGCs (Figures 5B–5D). First, the conductances rather than the cell type they were injected into dominated the kinetics of the STAs—i.e., a foveal and a peripheral MGC injected with the same conductances responded similarly (Figure 5B). Second, STA kinetics were similar with and without the inhibitory conductance, providing direct evidence that inhibitory synaptic input to the MGC did not regulate response kinetics (Figure 5B). Third, the spike rate and STA amplitude were both larger in the absence of the inhibitory conductance (Figures 5C and 5D).

These results indicate that inhibitory input acts to regulate gain but not kinetics of the responses of peripheral MGCs. Peripheral MGCs, unlike those in the fovea, receive input from multiple cones and hence may require gain regulation via inhibitory input to extend the range of contrasts they can encode (see Discussion).

Presynaptic Inhibition Does Not Shape the Excitatory Inputs of Foveal MGCs

The gradient in MGC response kinetics across retinal regions could, alternatively, be created by differences in kinetics of excitatory synaptic inputs onto MGCs. Consistent with this possibility, the kinetics of the linear filters (analogous to the STAs) characterizing the MGC excitatory synaptic inputs depended strongly on eccentricity (Figures 6A and 6B). The kinetics of linear filters for peripheral MGCs were similar to the corresponding STAs (Figures 6A–6C), which reaffirms the conclusion that postsynaptic inhibition is unlikely to play a significant role in temporal filtering of MGCs responses. These results suggest that a mechanism upstream of the MGCs creates the kinetic differences in retinal output across eccentricity.

Several mechanisms can shape the excitatory input to MGCs. Presynaptic inhibition, for example, could act on the axon terminals of midget bipolar cells (MBCs) that provide the dominant excitatory input to MGCs (Calkins et al., 1994; Kolb and Marshak, 2003). To

assess the contribution of presynaptic inhibition, we measured the effect of suppressing GABA and glycine receptor activity on excitatory synaptic inputs to foveal and peripheral MGCs. Suppressing inhibitory receptors substantially altered excitatory inputs and spike outputs of peripheral MGCs, including revealing a large response at light offset in addition to the normal response at light onset (Figures 6F and 6H). The extent of these changes precluded an estimate of the impact of presynaptic inhibition on response kinetics. The same manipulation had little or no effect on amplitude and kinetics of the foveal MGC excitatory input and spike output (Figures 6D, 6E and 6G). Thus, neither pre- nor post-synaptic inhibition substantially shapes the kinetics of responses of foveal MGCs.

Cone Photoreceptors Exhibit Slower Kinetics in the Fovea than the Periphery

Differences in the kinetics of responses of foveal and peripheral MGCs could originate in the cones themselves (Seiple and Holopigian, 1996; Tyler, 1985). Foveal and peripheral cones differ dramatically in density and morphology (Wikler et al., 1990). The cone density decreases with distance from the fovea and is 100-fold less in the peripheral retina (Wikler et al., 1990). Cones in the fovea have axons that extend ~400 μm in length, whereas central and peripheral cones have much shorter axons (Hsu et al., 1998). Foveal cones also have longer inner and outer segments compared to central and peripheral cones (Polyak, 1941, 1957). However, the possibility that cones could differ functionally across retinal location has not been tested.

To compare the kinetics of responses of foveal and peripheral cones, we recorded cone inner segment voltages in response to Gaussian noise stimuli and computed the linear filters—i.e., the filters that transform visual inputs into changes in cone voltage (Figure 7A; stimuli and analysis were identical to those used for the MGC responses in Figures 1 and 2 and 6). We focused on long (L) and middle (M) wavelength sensitive cones, identified based on their distinct spectral sensitivities. Surprisingly, the light-dependent voltage changes of foveal L and M cones were considerably slower than those of peripheral cones (Figure 7B). Voltage changes elicited by brief light flashes exhibited similar differences (Figure 7C). These differences are comparable in magnitude to the differences observed in the MGC responses —i.e., the time to peak of both the cone and MGC responses are ~2-fold slower in the fovea than periphery.

The differences in kinetics of light-dependent voltage changes of foveal and peripheral cones could originate within the phototransduction process, from electrical properties of the inner segment, or from network interactions mediated by horizontal cells or gap-junctional coupling (Barrow and Wu, 2009; Endeman et al., 2012; Hornstein et al., 2005a; Hornstein et al., 2005b; Verweij et al., 2003). To test for contributions of inner segment conductances, we measured cone currents using voltage-clamp recordings. Voltage-clamp recordings suppress contributions of inner segment conductances, which are activated by voltage changes, and the contributions of membrane capacitance, which can slow changes in voltage. Cone capacitance, for example, could differ across eccentricity due to the longer axons of foveal cones compared to peripheral cones (Hsu et al., 1998). The kinetics of responses of foveal and peripheral cones differed in voltage-clamp recordings both for filters derived from responses to Gaussian noise (Figure 7D; polarity opposite to current clamp recordings in

Figures 7B and C) and flash responses (not shown). Response differences were quantitatively very similar to those measured for voltage responses (i.e., in current-clamp recordings; Figures 7B and 7C). Current-clamp responses (Figures 7B and 7C) were slightly slowed compared to voltage-clamp responses (Figure 7D), likely due to membrane capacitance. The persistence of the differences in the kinetics of foveal and peripheral cone responses under voltage clamp (Figure 7D) indicates that they are not due to inner segment conductances.

Network interactions, as mentioned above, could also vary across retinal regions and hence contribute to differences in the kinetics of cone responses across eccentricity. To test for a contribution of horizontal cell feedback to cones, we suppressed horizontal cell responses with the AMPA-receptor antagonist NBQX (Dunn et al., 2007). Voltage responses of foveal and peripheral cones changed little following suppression of horizontal cell activity (Figures 7E and 7F). This is consistent with work indicating that horizontal cell feedback modulates a conductance with a reversal potential close to the cone photoreceptor resting potential, and hence impacts transmitter release more noticeably than the cone light response (Endeman et al., 2012; Verweij et al., 2003). To test for a role of gap junctions, we performed voltage clamp recordings from foveal cones after omitting ATP and GTP from the intracellular solution. Omission of ATP and GTP suppresses the phototransduction cascade causing the cGMP-gated channels to close in the recorded cone while retaining contributions from neighboring (coupled) photoreceptors. This manipulation strongly suppresses light responses in peripheral cones (Angueyra and Rieke, 2013). To further attenuate phototransduction, we included a poorly hydrolyzed GTP analog, GTPγS (Sampath and Rieke, 2004) in the intracellular solution during voltage clamp recordings from foveal cones. We also eliminated horizontal cell feedback by bath application of NBQX (Figure S7). These manipulations strongly suppressed light responses of foveal cones (Figure S7). The sensitivity of the light response to suppression of phototransduction suggests a small contribution of gap junctions between cone photoreceptors.

These experiments collectively suggest that the dramatic kinetic differences between foveal and peripheral cones originate from differences in the phototransduction process in the cone outer segment.

DISCUSSION

Despite the importance of the fovea for how we see, we know very little about the cellular and synaptic basis of its operation. Here, we reveal two important features that distinguish signaling in the fovea from that in the peripheral retina. First, a combination of intracellular recordings and structure-function analyses show that foveal MGCs receive minimal inhibitory synaptic input. This is unlike peripheral MGCs, which receive abundant inhibitory input. Second, we find that the responses of the very first retinal neurons—the cone photoreceptors—differ dramatically between the foveal and peripheral retina. These results, detailed below, provide a glimpse into the mechanistic specializations of the fovea, and provide a simple explanation for foveal/peripheral differences in sensitivity to rapidly-varying light inputs.

A Unique Mode of Synaptic Integration by Foveal MGCs

Understanding how excitatory and inhibitory inputs are integrated to shape neural responses is an extremely active research area (reviewed by Isaacson and Scanziani, 2011). Most circuits operate in a mode in which inhibition and excitation are balanced (I/E balance), and signaling relies on a momentary imbalance of the two.

Given the general importance of I/E balance, we were surprised to find that responses of MGCs in the primate fovea were minimally shaped by either pre- or post-synaptic inhibition. Foveal MGCs are unique in receiving input from single cone photoreceptors, and integration without inhibition ensures that cone signals are minimally altered before transmission to cortical neurons. The lack of inhibitory input is not shared by all foveal ganglion cell types. Thus, parallel and intertwined circuits in the fovea exhibit very different modes of synaptic integration. This physiological observation had a direct anatomical correlate (see below) and has important implications for the sophistication of foveal computations.

Integration of excitatory and inhibitory signals shapes computations performed by most sensory and cortical circuits—including feature selectivity, gain control, and coincidence detection (reviewed by Isaacson and Scanziani, 2011). A theme of recent retinal work has been the surprising computational specializations of non-foveal retinal circuits (Baccus et al., 2008; Buldyrev and Taylor, 2013; Farrow et al., 2013; Manookin et al., 2008; Münch et al., 2009; Sivyer et al., 2010; Venkataramani and Taylor, 2010; Venkataramani et al., 2014; Wei et al., 2011; Yonehara et al., 2011). These computations rely on synaptic inhibition generated by the diverse population of inner retinal amacrine cells (Farrow et al., 2013; Münch et al., 2009; Protti et al., 2014; Venkataramani et al., 2014; Wei et al., 2011; Yonehara et al., 2011). Our work here shows that this picture does not apply to computations by foveal MGCs. Instead, the reduced mechanistic repertoire shaping responses of foveal MGCs suggests that they lack the computational sophistication of their peripheral or wide-field counterparts. This distinction will be an important consideration in how visual computations are partitioned between retinal and cortical circuits in the fovea and periphery and between different foveal ganglion cell types.

Low Level of Expression of Inhibitory Receptors by Foveal MGCs Supports Unique Mode of Synaptic Integration

Foveal MGCs not only received minimal light-driven inhibitory input, but also expressed very few inhibitory receptors compared to excitatory receptors (low I/E ratio, see Figure 4). This was surprising given the higher I/E synapse ratios estimated previously from counts of ribbon and non-ribbon synapses onto foveal MGC dendrites using electron microscopy (Calkins et al., 1994; Calkins and Sterling, 1996; Kolb and Dekorver, 1991). These two types of experiments, however, measure different anatomical aspects of the synapses and hence are not necessarily contradictory.

Several issues could contribute to this difference, including (1) non-ribbon excitatory synapses, (2) differences in synaptic structure, and (3) postsynaptic receptors. Amacrine synapses were identified in electron microscopy studies based on the absence of ribbons (Calkins et al., 1994). MGCs could receive non-ribbon excitatory contacts, e.g., from

glutamatergic amacrine cells (Lee et al., 2014; Marshak et al., 2015), and bipolar cells could make some conventional synapses on the dendrites of MGCs (Kolb and Dekorver, 1991). The MGC is contacted by a single midget bipolar cell with a claw-like synaptic terminal containing 25–50 ribbons (Calkins et al., 1994) packed into a small volume (~70 μm^3). This is akin to the giant mossy fiber bouton contacting the CA3 pyramidal neuron (Bischofberger et al., 2006), a very robust excitatory synapse. The unusual anatomy of the bipolar-MGC synapse may produce stronger excitatory synaptic input to the MGC that cannot be inferred by counting synapses. Postsynaptic receptor densities at individual amacrine and bipolar synaptic contacts could differ. The differences we observe in dendritic volume occupancy of inhibitory and excitatory receptors support this possibility. However, we were not able to measure the size of the receptor clusters with confidence due to the limited resolution of light microscopy. Development of techniques that allow the simultaneous labeling of excitatory and inhibitory receptors on MGC dendrites at electron microscopy resolution could provide the needed estimates of receptor cluster size. Independent of the reason, the functional I/E ratios correlated more strongly with I/E ratios based on receptor expression than counts of presynaptic structures. This is an important result given the vast amount of electron microscopy data available now and in the near future and the desire to draw functional inferences from these data.

In many neural circuits, including the peripheral retina, inhibitory interneurons establish synapses before primary excitatory neurons (Ben-Ari, 2014; Hendrickson, 1994, 1996; Hoon et al., 2014). Interestingly, foveal synapses develop in the opposite sequence: excitatory ribbon synapses between bipolar cells and ganglion cells form prior to amacrine inhibitory synapses (Hendrickson, 1994, 1996; Hoon et al., 2014). This sequence suggests that the foveal midget circuitry from its inception is wired such that the excitatory input from single cones dominates synaptic integration.

A Simple yet Surprising Mechanistic Link to Human Perception

A wealth of human psychophysical experiments have shown that sensitivity to rapidly varying light inputs is higher in the periphery than in the fovea (Rovamo and Raninen, 1988; Tyler, 1985; Waugh and Hess, 1994). This difference is not subtle: the estimated time constant based on human perception differs ~2-fold for foveal and peripheral vision (Tyler, 1985). The reduced temporal sensitivity of foveal vision is an important consideration in the design of devices such as visual displays and will be an important consideration for visual prosthetics.

We were surprised to find that differences in inhibitory synaptic input to foveal and peripheral MGCs contributed minimally to differences in temporal sensitivity. Instead, post-synaptic inhibition controls the gain of peripheral MGC responses. This form of gain control may be needed in the periphery, where visual signals are pooled from several cone photoreceptors, but not in the fovea where MGCs receive (indirect) input from single cones.

Differences in temporal sensitivity could instead be explained by differences in the kinetics of the responses of the cone photoreceptors themselves. Indeed, responses of foveal cones were slower than those of peripheral cones. Importantly, cone photoreceptor responses (Figure 7), ganglion cell responses (Figure 1 and Solomon et al., 2002) and perception

(Tyler, 1985) all show a near-identical 2-fold difference in kinetics between the fovea and periphery. The similarity of these measures suggests that the cones themselves account for the well-established foveal/peripheral differences in sensitivity to rapid variations in light inputs. Consequently, foveal cones integrate their inputs over longer times—reducing sensitivity to rapidly-varying inputs while improving sensitivity to slowly-varying inputs. Peripheral cone circuits, in which MGCs receive input from multiple cones, improve sensitivity by averaging across multiple converging cones (Goodchild et al., 1996), and this spatial integration may obviate the need for temporal integration in the cones themselves.

Differences in the kinetics of foveal and peripheral cone responses appear to originate within the phototransduction cascade rather than from inner segment or network effects. These differences may complement anatomical differences between the cones (Tyler, 1985). For instance, the axons of foveal cones are ~10-fold longer than those of peripheral cones; the slower kinetics of foveal cone responses may be matched to the filtering associated with propagation of signals down their long axons (Hsu et al., 1998).

In summary, our study builds on previous studies in retina and human perception in the following ways: (1) Functional recordings from MGCs in the fovea allowed us to directly measure light-driven excitatory and inhibitory synaptic inputs to the MGCs and reveal a unique mode of synaptic integration without inhibition. (2) Anatomical analyses show that foveal MGCs express few inhibitory receptors compared to their peripheral counterparts, corroborating the physiological findings. (3) Comparison of responses of foveal and peripheral cone photoreceptors revealed a surprising 2-fold difference in kinetics and a simple explanation for the lower temporal sensitivity of foveal vision.

STAR ★ METHODS

KEY RESOURCES TABLE

REAGENT or RESOURCE	SOURCE	IDENTIFIER
Antibodies		
Goat polyclonal anti-GluA3	Santa Cruz Biotechnology	Cat#: sc7613
Mouse monoclonal anti-Gephyrin	Synaptic Systems	Clone mab3b11, cat#147 111
Mouse monoclonal anti-$GABA_A\alpha1$	Millipore	Clone mab339, cat# 2090441
Rabbit polyclonal anti-$GABA_C\rho$	R. Enz/H. Wassle	N/A
Donkey polyclonal anti-goat Alexa Fluor 647	Jackson ImmunoResearch	Code: 705-605-147
Donkey polyclonal anti-mouse Alexa Fluor 488	Jackson ImmunoResearch	Code: 715-545-150
Donkey polyclonal anti-rabbit Alexa Fluor 488	Jackson ImmunoResearch	Code: 711-545-152
Donkey polyclonal anti-mouse Alexa Fluor 647	Jackson ImmunoResearch	Code: 715-605-150

Streptavidin Alexa Fluor 568 conjugate	Invitrogen molecular probes	Cat#: S11226
Biological Samples		
Macaque retina	Regional Primate Research Centre	N/A
Chemicals, Peptides, and Recombinant Proteins		
Ames	Sigma	1420
GABAzine	Sigma	SR-95531
TPMPA	Tocris	1040
Strychnine	Sigma	S8753
MNI-glutamate	Tocris	1490
RuBi-GABA	R&D Systems	3400
NBQX	Tocris	1044
Neurobiotin	Vector Labs	SP1120
Gold Particles/micro carriers (1.6μm diameter)	Bio-Rad	Cat#: 165-2264
Vectashield Antifade mounting medium	Vector Labs	CatN: H-1000
GTPγS	Sigma	G8634
Recombinant DNA		
pcDNA-tdTomato	R. Wong, University of Washington Morgan et al., 2008	N/A
pcDNA-PSD95CFP	Construct modified from PSD95-YFP construct from A.M. Craig, University of British Columbia Kerschensteiner et al., 2009	N/A
pcDNA-PSD95YFP	A.M. Craig, University of British Columbia Morgan et al., 2008	N/A
pcDNA- $GABA_A$α1-YFP	This paper (construct modified from $GABA_A$α1-pHGFP construct from T. Jacobs, University of Pittsburgh)	N/A
pcDNA- $GABA_A$γ2	A.M. Craig, University of British Columbia	N/A
pcDNA- $GABA_A$β2/3	A.M. Craig, University of British Columbia	N/A
Software and Algorithms		

IGOR Pro	WaveMetrics	https://www.wavemetrics.com/
MATLAB	Mathworks	http://ch.mathworks.com/products/matlab
Symphony	Symphony-DAS	https://github.com/symphony-das
ImageJ NIH		https://imagej.nih.gov/ij/
Amira FEI	Visualization Sciences Group	https://www.fei.com/software/amira-3d-for-life-sciences/
MetaMorph	Molecular Devices	https://www.moleculardevices.com/

CONTACT FOR REAGENT AND RESOURCE SHARING

Further information and requests for resources and reagents should be directed to the Lead Contact Fred Rieke (rieke@uw.edu).

EXPERIMENTAL MODEL AND SUBJECT DETAILS

Retinas from both male and female Macaques (*M. mulatta, M. nemestrina*, and *M. fascicularis*) aged between 4–21 years old were obtained through the Tissue Distribution Program of the Regional Primate Research Center at the University of Washington following procedures approved by the Institutional Animal Care and Use Committee. Animals were housed in primate center facilities, cared for by their veterinary staff and were in good health. For each dataset, we collected data from at least 3 retinas from at least 3 animals.

METHOD DETAILS

Tissue Preparation and Cell Identification—Electrical recordings from foveal (<1 mm from foveal pit), central (2–4 mm from foveal pit) and peripheral (>6 mm from foveal pit) primate retina followed approaches used previously for peripheral retinal recordings (Cafaro and Rieke, 2013). For all recordings, a piece of retina was isolated from the choroid and pigment epithelium and mounted flat in a recording chamber. The retina was mounted ganglion cell side up for ganglion cell recordings and photoreceptor side up for cone recordings. The retina was superfused with warmed (31–34°C) and oxygenated (5% CO_2/95% O_2) Ames solution (Sigma). The foveal pit was clearly identifiable when focusing on the cone array (Figure 1).

All functional recordings were performed at a background light level of ~4,000 absorbed photons per cone per sec (R*/cone/s). Responses in the rods themselves were saturated at 10-fold lower light levels (data not shown), and hence the rods should contribute minimally to the reported ganglion cell or cone responses. Of note, the density of rod photoreceptors, which are abundant in central and peripheral retina, drops precipitously near the fovea—in fact, the central fovea (<0.3 mm from the foveal center) is devoid of rods altogether and has the highest cone density (Kolb et al., 2002; Wässle et al., 1995).

MGCs were initially identified based on their relatively sustained responses to light steps compared to the more transient responses of wide-field ganglion cells (Cafaro and Rieke, 2013; De Monasterio and Gouras, 1975). In central and peripheral retina identification was aided by the morphology and size of the MGC somas (Crook et al., 2011; Dacey, 1993; Kolb

and Marshak, 2003). Cell identification was confirmed by fluorescence imaging (using Neurobiotin or Alexa 594 dye) as shown in Figure 1. The foveal MGCs have a characteristic small dendritic arbor of 5–10 μm (Figure 1) compared to ~20 μm arbors of foveal wide-field ganglion cells (Figure 4).

The baseline spike rate of MGCs at the three retinal locations at a mean luminance of 4,000 R*/cone/s ranged from ~5–30 Hz. Before initiating data collection, the sensitivity of the retina was determined from the spike responses of MGCs to a full field 100% contrast light step from a background of ~4,000 R*/cone/s. Data were collected from cells in which this stimulus produced a peak increase in firing rate of >40 spikes/s in foveal and central retina and >100 spikes/s in the peripheral retina. This contrast gain—i.e., 0.4 spikes/% contrast—is within a factor of 2 of contrast gains from in vivo recordings of foveal MGCs at similar mean light levels (Benardete and Kaplan, 1999a, b; Kaplan and Benardete, 2001; Kaplan and Shapley, 1986; Lee et al., 1990; Purpura et al., 1988; Solomon et al., 2002). Recordings from the fovea were pooled across both L and M-cone driven ON-type MGCs. OFF-type MGCs occurred far less frequently near the top of the ganglion cell layer in the fovea (Yin et al., 2014); this restricted our ability to collect extensive data from foveal OFF MGCs and hence we report results predominantly from ON MGCs.

Light Stimulation—Light stimuli were delivered from LEDs with peak spectral outputs at 470 nm or 640 nm. The stimuli were delivered through the microscope condenser and glass bottom of the recording chamber. Light intensities are reported as isomerizations per cone per second (R*/cone/s), calculated using the calibrated LED and spectra, the photoreceptor spectral sensitivity (Baylor et al., 1987), and assumed a cone collecting area of 0.37 μm^2 (Schnapf et al., 1990). Full-field stimuli covered a 500-μm-diameter spot on the retina centered on the cell of interest. The spot size covered both the center and most of the surround of the MGC receptive field at each of the retinal locations. Gaussian noise stimuli had 50% contrast (SD/mean) and 0–60 Hz bandwidth. To analyze responses to these stimuli, we computed the average stimulus preceding an action potential (the spike-triggered average or STA) or the corresponding linear filter for ganglion cell excitatory synaptic currents and cone photovoltages/photocurrents.

Voltage-Clamp and Conductance Measurement—Whole-cell patch-clamp recordings were made using a Multiclamp 700B amplifier (Molecular Devices). Pipettes for voltage-clamp recordings were filled with a Cs-based internal solution containing (in mM): 105 Cs methanesulfonate, 10 TEA-Cl, 20 HEPES, 10 EGTA, 5 Mg-ATP, 0.5 Tris-GTP, and 2 QX-314, pH ~7.3, ~280 mOsm. An inhibitory cocktail (20 μM GABAzine, 50 μM TPMPA and 2 μM strychnine; Tocris) was added to the perfusion solution to block $GABA_{A,}$ $GABA_C$ and glycine receptors as indicated in Figures 2 and 6 and Figure S5. Voltage-clamp recordings were made using pipettes of 5 ΩU resistance for ganglion cells and of 10–14 MΩ resistance for cones. Whole-cell patch clamp recordings were performed from the inner segments of cone photoreceptors as described previously (Angueyra and Rieke, 2013). The internal solution contained (in mM): 133 potassium aspartate, 10 KCl, 10 HEPES, 1 $MgCl_2$, 4 ATP, 0.5 GTP, pH ~7.3, ~280 mOSM (Angueyra and Rieke, 2013). For cone recordings in Figure 7E and 7F, 10 μM NBQX (Tocris) was added to the bath perfusion solution. GTPγS

(Sigma) was added at a concentration of 50 μM to the intracellular solution (Figure S7). Unless specified otherwise, reported voltages have been corrected for a −10 mV liquid junction potential.

The resting membrane potential of foveal MGCs was ~−55mV, similar to that of peripheral MGCs. For measurements of excitatory and inhibitory synaptic currents, cells were voltage-clamped at several holding potentials between −80 and +30 mV. Light steps were delivered while excitatory and inhibitory reversal potentials were assessed empirically by focusing on time points dominated by either excitatory or inhibitory input, and identifying holding potentials that minimized each (near −60 and +10 mV). The cell was held at the estimated excitatory reversal potential when inhibitory currents were recorded and at the estimated inhibitory reversal potential when excitatory currents were recorded. For measurement of current-voltage curves (see Figure S5), light stimuli were delivered starting 1–2 s after a voltage step to allow any transient change in current to subside.

Spontaneous IPSCs were apparent immediately after depolarizing a MGC to the reversal potential for excitatory input, and spontaneous IPSCs were stable in amplitude throughout the time the cell remained depolarized (as much as 20 min in some cases; Figure S5). Thus changes in intracellular chloride following depolarization did not appear to attenuate inhibitory currents. Spontaneous IPSCs in foveal and peripheral MGCs had similar amplitudes and kinetics (Figure S5C).

Caged Compounds—MNI-glutamate (2 mM, Tocris Biosciences) and RuBi-GABA (5–10 μM, R&D Systems) were puffed onto the tissue from a glass pipette. Photolysis of MNI-glutamate and RuBi-GABA was performed with light from a mercury arc lamp (X-cite, Excelitas Technologies). Light was delivered to the entire tissue in 50 ms pulses through the data-acquisition software (Symphony, Symphony-DAS, Seattle, USA). MGCs were identified based on their spike responses as shown in Figure 1 for fovea and periphery. Light-evoked responses were blocked by perfusing with a solution containing cadmium chloride (200 μM). Responses to uncaged GABA and glutamate were measured at the excitatory and inhibitory reversal potentials. A limitation in quantitative interpretation of these experiments is that previous studies have shown that MNI-Glutamate can inhibit GABA receptors (Fino et al., 2009; Maier et al., 2005). This could explain why the amplitude of GABA-mediated current is smaller than expected from the immunohistochemical analysis for both foveal and peripheral MGCs. Nonetheless, the relative amplitude of inhibitory to excitatory current is larger for peripheral MGCs compared to their foveal counterparts, consistent with the rest of our experiments.

Dynamic Clamp—Synaptic input was mimicked and manipulated during dynamic clamp experiments (Cafaro and Rieke, 2013). Cells were current-clamped using pipettes filled with a K-based internal solution (containing, in mM: 122 K-Aspartate, 10 KCl, 1 CaCl2, 1 MgCl, 2 EGTA, 10 HEPES, 4 Mg-ATP, and 0.5 Tris-GTP, pH 7.2 with KOH, 280 mOsm). Current injected into a cell (I) during dynamic clamp experiments was calculated as

$$I(t) = G_{\mathrm{exc}}(t)\,(\mathrm{V}(\mathrm{t}-\Delta t) - E_{exc}) + G_{\mathrm{inh}}(t)\,(V(t-\Delta t) - E_{\mathrm{inh}}) \quad (1)$$

where G_{exc} and G_{inh} are the conductances recorded during light stimulation, V is the membrane potential, and E_{exc} (E_{inh}) is the reversal potential for excitatory (inhibitory) synaptic input. Current injected at time t was calculated from the measured voltage at time t −Δt, with Δt = 100 μs. E_{exc} was 0 mV and E_{inh} was −90 mV. Excitatory and inhibitory synaptic conductances in response to Gaussian noise stimuli were measured near-simultaneously from peripheral MGCs using an alternating voltage approach (Cafaro and Rieke, 2010). The excitatory conductances from a foveal MGC to similar light stimuli were used for the dynamic clamp experiments. Upon initiating a dynamic clamp experiment, the amplitudes of the excitatory and inhibitory conductances were scaled by a common factor, while keeping their ratio constant, to achieve spike numbers near those recorded during light stimulation. As needed, a modest constant current (< 100 pA) was injected to maintain a spontaneous firing rate of 5 – 20 spikes/s.

The dynamic clamp approach described in Equation 1 neglects the NMDA conductances that are present in the inputs to MGCs. Previous studies have shown that NMDA conductances, however, have little impact on peripheral MGCs' spike responses under the conditions of our experiments (Cafaro and Rieke, 2013). Block of NMDA receptors with L-AP4 similarly had little effect on the spike responses of foveal MGCs to Gaussian noise stimuli (data not shown).

The STAs in Figure 5C are one component of a linear-nonlinear (LN) model. A change in the amplitude of the STA corresponds to a change in the x axis scaling of the static nonlinearity (Chichilnisky, 2001; Kim and Rieke, 2001). To compare STA amplitudes, the x-axes of the nonlinearities were scaled to produce maximal overlap and the STA amplitudes correspondingly adjusted. This associates any change in response with a change in the STA.

Immunohistochemistry—MGCs were filled intracellularly with a solution containing 5 mM neurobiotin and retinas were immersion fixed for either 15 min (for GluA3, $GABA_A\alpha1$ and gephyrin labeling) or 30 min (for $GABA_C$ labeling) with 4% paraformaldehyde in 0.1M phosphate buffered saline (PBS, pH 7.4). Post-fixation the tissue was washed in PBS and then freeze-cracked in 30% sucrose (made in PBS) to facilitate antibody penetration. Antibody incubation was carried out in a blocking solution containing 5% donkey serum and 1% triton (Sigma) in PBS for 1 week at 4°C. Antibodies used were directed against the GluA3 subunit of AMPA receptor (goat polyclonal, 1:500, Santa Cruz Biotechnology), Gephyrin (mouse monoclonal mab3b11, 1:1000, Synaptic Systems), $GABA_A$ receptor α1 subunit (mouse monoclonal mab339, 1:500, Millipore). As a control for non-specific association of the receptor signal within MGC dendrites, we labeled for $GABA_c$ receptors (Enz et al., 1996) using an antibody against $GABA_C$ receptor ρ subunit (rabbit polyclonal, 1:500, kindly provided by R. Enz and H. Wässle), known to localize at bipolar cell terminals, and found negligible amounts on MGC dendrites (Figure S6). Secondary antibodies were anti-isotypic Alexa Fluor conjugates (1:1000, Invitrogen or Jackson ImmunoResearch). Secondary antibody incubation was carried out in blocking solution for 3–4 hr at room temperature, and after washes in PBS the retinas were subsequently mounted in Vectashield (Vector labs). To amplify the neurobiotin signal, streptavidin conjugated to Alexa Fluor 568 (1:1000, Invitrogen) was included with the secondary antibody.

Biolistic Transfection—Gold particles (1.6 μm diameter; 12.5 mg; Bio-Rad) were coated with DNA plasmids encoding tdTomato (24 μg), PSD95-CFP or PSD95-YFP (12 μg), $GABA_A\alpha1$-YFP (modified version of $GABA_A\alpha1$ tagged fusion constructs (Connolly et al., 1996; Jacob et al., 2008)—a generous gift from T. Jacobs) (19 μg), $GABA_A\gamma2$ (20 μg) and $GABA_A\beta2/3$ (19 μg) under the control of the cytomegalovirus promoter. The particles were delivered to retinal ganglion cells in whole-mount retinas using a Helios gene gun (Bio-Rad). Organotypic culturing and transfection of retinas was performed as described previously (Lye et al., 2007; Percival et al., 2014). In brief, pieces of retina were mounted ganglion cell side up onto a 0.4 μm Millicell tissue culture inset (Millipore). Transfected retinas were incubated in a 95% O_2/5% CO_2 environment for at least two days in sterile Ames medium at 32°C. The retinas were then immersion fixed in 4% paraformaldehyde and mounted on glass slides directly or used for immunostaining.

Imaging and Analysis—Image stacks of whole mounted retinas were acquired on an Olympus FV1000 laser scanning confocal microscope. The tissue was imaged using a 1.35 NA 60X oil immersion objective at a xyz voxel size of 0.069, 0.069, 0.3 μm. For acquiring overview images, a 0.85 NA 20X oil immersion objective was used. Each optical plane was averaged three to four times (Kalman filter). Raw image stacks were processed using MetaMorph (Molecular Devices) and Amira (FEI Visualization Sciences Group). All acquired images were median filtered in MetaMorph before their 3D visualization in Amira.

To quantify the percentage occupancy of receptor signal with the MGC dendritic mask, the dendrites of the MGC were at first masked in 3-dimensions using the *Labelfield* function in Amira such that pixels outside the mask were set to a value of zero. The MGC dendritic mask was multiplied by the receptor (GluA3, PSD95, Gephyrin or $GABA_A\alpha1$) channel to isolate the receptor signal exclusively within the dendritic mask. A constant threshold at 4 standard deviations above the noise peak (see Figure S3) was selected to exclude background fluorescence and retain only pixels representing the signal (e.g., receptors). The threshold was chosen by fitting the distribution of pixel values for each immunolabeling with a gamma distribution to determine the peak and standard deviation of the noise (background) pixels (Figure S3). The volume of the receptor pixels above the threshold was expressed as a percentage of the total volume occupied by the pixels within the MGC dendritic mask.

To assess if the low I/E ratio in foveal MGCs is due to a lower overall amount of inhibitory receptor protein expression in foveal MGCs rather than size differences between foveal and peripheral MGC dendritic arbors, we compared the volume occupancy of the receptor signal of peripheral MGCs in the entire dendritic arbor with the receptor occupancy estimated in smaller stretches of peripheral MGC dendritic volume (70 μm^3) comparable to the arbor of foveal MGCs (Figure S1). The anatomical I/E ratio for peripheral MGCs was similar in both cases (full arbor versus smaller volume), indicating that the low I/E ratio of inhibitory receptors in foveal MGCs is not merely due to the foveal MGC dendritic arbor being smaller than the dendritic arbor for peripheral MGCs.

To assess the % colocalization between PSD95-YFP and GluA3 immunolabeling or $GABA_A$-YFP clusters and Gephyrin immunolabeling (see Figure S1), PSD95-YFP or

$GABA_A$-YFP signal within the MGC dendritic mask was first isolated using the Amira software as described above. Thereafter, PSD95-YFP or $GABA_A$-YFP clusters were assessed for colocalization with GluA3 or Gephyrin immunolabeling respectively using a custom written MATLAB (Mathworks, USA) routine. GluA3 and Gephyrin signals were thresholded (similar to thresholds set in Figure S3) to exclude background fluorescence. For each PSD95-YFP punctum within the MGC dendrite the proportion of PSD95 pixels that also contain GluA3 signal was determined. Similarly, for each $GABA_A$-YFP punctum the proportion of $GABA_A$ pixels that also contain Gephyrin signal was determined. A PSD95 punctum was considered as "colocalized" with the GluA3 signal, if the GluA3 signal occupied more than 20% of all the pixels representing the PSD95 punctum. Scoring for all the PSD95 puncta yielded a % colocalization (Figure S1). The % of $GABA_A$-YFP clusters colocalized with Gephyrin was calculated the same way (Figure S1). As a control, the GluA3 or Gephyrin channel were flipped 90°and their % colocalization with PSD95-YFP and $GABA_A$-YFP clusters determined (Figure S1).

QUANTIFICATION AND STATISTICAL ANALYSIS

We used the nonparametric Wilcoxon-Mann-Whitney rank sum test for all the statistical analysis. Error bars indicate SD. Statistical parameters including the exact value of n, precision measures (mean ± SD) and statistical significance are reported in the figures and in the figure legends (see individual sections). The significance threshold was placed at $\alpha = 0.05$ (n.s., $p > 0.05$; *, $p < 0.05$; **, $p < 0.01$; ***, $p < 0.001$).

Supplementary Material

Refer to Web version on PubMed Central for supplementary material.

Acknowledgments

We thank E.J. Chichilnisky, G. Horwitz, G.D. Field and J.M. Angueyra for helpful comments. We would like to thank C. Puller for helpful discussions and suggestions. We thank R. Enz and H. Wässle for the $GABA_C$ antibody, T. Jacob for the $GABA_A\alpha1$-fluorescent protein construct and T. Yoshimatsu for generating the $GABA_A\alpha1$-YFP fusion construct. We thank M. Cafaro, S. Cunnington, and P. Newman for excellent technical assistance. This work is supported by the Human Frontier Science Foundation (long-term fellowship to R.S.), Knights Templar Eye Foundation (career starter grant to M.H.), ARCS foundation (J.B.), HHMI (F.R.) and NIH grants (EY026070 to R.S., EY11850 to F.R. and EY10699 to R.O.W.).

References

Abbott CJ, Percival KA, Martin PR, Grünert U. Amacrine and bipolar inputs to midget and parasol ganglion cells in marmoset retina. Vis Neurosci. 2012; 29:157–168. [PubMed: 22564345]

Angueyra JM, Rieke F. Origin and effect of phototransduction noise in primate cone photoreceptors. Nat Neurosci. 2013; 16:1692–1700. [PubMed: 24097042]

Asari H, Meister M. Divergence of visual channels in the inner retina. Nat Neurosci. 2012; 15:1581–1589. [PubMed: 23086336]

Baccus SA, Olveczky BP, Manu M, Meister M. A retinal circuit that computes object motion. J Neurosci. 2008; 28:6807–6817. [PubMed: 18596156]

Barrow AJ, Wu SM. Low-conductance HCN1 ion channels augment the frequency response of rod and cone photoreceptors. J Neurosci. 2009; 29:5841–5853. [PubMed: 19420251]

Baylor DA, Nunn BJ, Schnapf JL. Spectral sensitivity of cones of the monkey Macaca fascicularis. J Physiol. 1987; 390:145–160. [PubMed: 3443931]

Ben-Ari Y. The GABA excitatory/inhibitory developmental sequence: a personal journey. Neuroscience. 2014; 279:187–219. [PubMed: 25168736]

Benardete EA, Kaplan E. The dynamics of primate M retinal ganglion cells. Vis Neurosci. 1999a; 16:355–368. [PubMed: 10367969]

Benardete EA, Kaplan E. Dynamics of primate P retinal ganglion cells: responses to chromatic and achromatic stimuli. J Physiol. 1999b; 519:775–790. [PubMed: 10457090]

Bischofberger J, Engel D, Frotscher M, Jonas P. Timing and efficacy of transmitter release at mossy fiber synapses in the hippocampal network. Pflugers Arch. 2006; 453:361–372. [PubMed: 16802161]

Buldyrev I, Taylor WR. Inhibitory mechanisms that generate centre and surround properties in ON and OFF brisk-sustained ganglion cells in the rabbit retina. J Physiol. 2013; 591:303–325. [PubMed: 23045347]

Cafaro J, Rieke F. Noise correlations improve response fidelity and stimulus encoding. Nature. 2010; 468:964–967. [PubMed: 21131948]

Cafaro J, Rieke F. Regulation of spatial selectivity by crossover inhibition. J Neurosci. 2013; 33:6310–6320. [PubMed: 23575830]

Calkins DJ, Sterling P. Absence of spectrally specific lateral inputs to midget ganglion cells in primate retina. Nature. 1996; 381:613–615. [PubMed: 8637598]

Calkins DJ, Sterling P. Microcircuitry for two types of achromatic ganglion cell in primate fovea. J Neurosci. 2007; 27:2646–2653. [PubMed: 17344402]

Calkins DJ, Schein SJ, Tsukamoto Y, Sterling P. M and L cones in macaque fovea connect to midget ganglion cells by different numbers of excitatory synapses. Nature. 1994; 371:70–72. [PubMed: 8072528]

Chichilnisky EJ. A simple white noise analysis of neuronal light responses. Network. 2001; 12:199–213. [PubMed: 11405422]

Connolly CN, Wooltorton JR, Smart TG, Moss SJ. Subcellular localization of gamma-aminobutyric acid type A receptors is determined by receptor beta subunits. Proc Natl Acad Sci USA. 1996; 93:9899–9904. [PubMed: 8790428]

Crook JD, Manookin MB, Packer OS, Dacey DM. Horizontal cell feedback without cone type-selective inhibition mediates “red-green” color opponency in midget ganglion cells of the primate retina. J Neurosci. 2011; 31:1762–1772. [PubMed: 21289186]

Dacey DM. The mosaic of midget ganglion cells in the human retina. J Neurosci. 1993; 13:5334–5355. [PubMed: 8254378]

De Monasterio FM, Gouras P. Functional properties of ganglion cells of the rhesus monkey retina. J Physiol. 1975; 251:167–195. [PubMed: 810576]

Dunn FA, Lankheet MJ, Rieke F. Light adaptation in cone vision involves switching between receptor and post-receptor sites. Nature. 2007; 449:603–606. [PubMed: 17851533]

Endeman D, Fahrenfort I, Sjoerdsma T, Steijaert M, Ten Eikelder H, Kamermans M. Chloride currents in cones modify feedback from horizontal cells to cones in goldfish retina. J Physiol. 2012; 590:5581–5595. [PubMed: 22890705]

Enz R, Brandstätter JH, Wässle H, Bormann J. Immunocytochemical localization of the GABAc receptor rho subunits in the mammalian retina. J Neurosci. 1996; 16:4479–4490. [PubMed: 8699258]

Farrow K, Teixeira M, Szikra T, Viney TJ, Balint K, Yonehara K, Roska B. Ambient illumination toggles a neuronal circuit switch in the retina and visual perception at cone threshold. Neuron. 2013; 78:325–338. [PubMed: 23541902]

Fino E, Araya R, Peterka DS, Salierno M, Etchenique R, Yuste R. RuBi-Glutamate: Two-Photon and Visible-Light Photoactivation of Neurons and Dendritic spines. Front Neural Circuits. 2009; 3:2. [PubMed: 19506708]

Fischer F, Kneussel M, Tintrup H, Haverkamp S, Rauen T, Betz H, Wässle H. Reduced synaptic clustering of GABA and glycine receptors in the retina of the gephyrin null mutant mouse. J Comp Neurol. 2000; 427:634–648. [PubMed: 11056469]

Goodchild AK, Ghosh KK, Martin PR. Comparison of photoreceptor spatial density and ganglion cell morphology in the retina of human, macaque monkey, cat, and the marmoset Callithrix jacchus. J Comp Neurol. 1996; 366:55–75. [PubMed: 8866846]

Grünert U, Greferath U, Boycott BB, Wässle H. Parasol (P alpha) ganglion-cells of the primate fovea: immunocytochemical staining with antibodies against GABAA-receptors. Vision Res. 1993; 33:1–14. [PubMed: 8383899]

Hecht S, Verrijp CD. Intermittent Stimulation by Light: Iii. The Relation between Intensity and Critical Fusion Frequency for Different Retinal Locations. J Gen Physiol. 1933; 17:251–268. [PubMed: 19872777]

Hendrickson AE. Primate foveal development: a microcosm of current questions in neurobiology. Invest Ophthalmol Vis Sci. 1994; 35:3129–3133. [PubMed: 8045707]

Hendrickson AE. Synaptic development in macaque monkey retina and its implications for other developmental sequences. Perspect Dev Neurobiol. 1996; 3:195–201. [PubMed: 8931093]

Hoon M, Okawa H, Della Santina L, Wong RO. Functional architecture of the retina: development and disease. Prog Retin Eye Res. 2014; 42:44–84. [PubMed: 24984227]

Hornstein EP, Verweij J, Li PH, Schnapf JL. Gap-junctional coupling and absolute sensitivity of Photoreceptors in macaque retina (vol 25, pg 11201, 2005). J Neurosci. 2005a; 25:11201–11209. [PubMed: 16319320]

Hornstein EP, Verweij J, Schnapf JL. Electrical coupling between red and green cones in primate retina. Invest Ophth Vis Sci. 2005b; 46

Hsu A, Tsukamoto Y, Smith RG, Sterling P. Functional architecture of primate cone and rod axons. Vision Res. 1998; 38:2539–2549. [PubMed: 12116702]

Isaacson JS, Scanziani M. How inhibition shapes cortical activity. Neuron. 2011; 72:231–243. [PubMed: 22017986]

Jacob TC, Moss SJ, Jurd R. GABA(A) receptor trafficking and its role in the dynamic modulation of neuronal inhibition. Nat Rev Neurosci. 2008; 9:331–343. [PubMed: 18382465]

Jadzinsky PD, Baccus SA. Transformation of visual signals by inhibitory interneurons in retinal circuits. Annu Rev Neurosci. 2013; 36:403–428. [PubMed: 23724996]

Kaplan E, Benardete E. The dynamics of primate retinal ganglion cells. Prog Brain Res. 2001; 134:17–34. [PubMed: 11702542]

Kaplan E, Shapley RM. The primate retina contains two types of ganglion cells, with high and low contrast sensitivity. Proc Natl Acad Sci USA. 1986; 83:2755–2757. [PubMed: 3458235]

Kerschensteiner D, Morgan JL, Parker ED, Lewis RM, Wong RO. Neurotransmission selectively regulates synapse formation in parallel circuits in vivo. Nature. 2009; 460:1016–1020. [PubMed: 19693082]

Kim KJ, Rieke F. Temporal contrast adaptation in the input and output signals of salamander retinal ganglion cells. J Neurosci. 2001; 21:287–299. [PubMed: 11150346]

Kolb H, Dekorver L. Midget ganglion cells of the parafovea of the human retina: a study by electron microscopy and serial section reconstructions. J Comp Neurol. 1991; 303:617–636. [PubMed: 1707423]

Kolb H, Marshak D. The midget pathways of the primate retina. Doc Ophthalmol. 2003; 106:67–81. [PubMed: 12675488]

Kolb H, Zhang L, Dekorver L, Cuenca N. A new look at calretinin-immunoreactive amacrine cell types in the monkey retina. J Comp Neurol. 2002; 453:168–184. [PubMed: 12373782]

Koulen P, Fletcher EL, Craven SE, Bredt DS, Wässle H. Immunocytochemical localization of the postsynaptic density protein PSD-95 in the mammalian retina. J Neurosci. 1998; 18:10136–10149. [PubMed: 9822767]

Lee BB, Pokorny J, Smith VC, Martin PR, Valberg A. Luminance and chromatic modulation sensitivity of macaque ganglion cells and human observers. J Opt Soc Am A. 1990; 7:2223–2236. [PubMed: 2090801]

Lee S, Chen L, Chen M, Ye M, Seal RP, Zhou ZJ. An unconventional glutamatergic circuit in the retina formed by vGluT3 amacrine cells. Neuron. 2014; 84:708–715. [PubMed: 25456497]

Lye MH, Jakobs TC, Masland RH, Koizumi A. Organotypic culture of adult rabbit retina. J Vis Exp. 2007; 3:190.

Maier W, Corrie JE, Papageorgiou G, Laube B, Grewer C. Comparative analysis of inhibitory effects of caged ligands for the NMDA receptor. J Neurosci Methods. 2005; 142:1–9. [PubMed: 15652611]

Manookin MB, Beaudoin DL, Ernst ZR, Flagel LJ, Demb JB. Disinhibition combines with excitation to extend the operating range of the OFF visual pathway in daylight. J Neurosci. 2008; 28:4136–4150. [PubMed: 18417693]

Marshak DW, Chuang AZ, Dolino DM, Jacoby RA, Liu WS, Long YE, Sherman MB, Suh JM, Vila A, Mills SL. Synaptic connections of amacrine cells containing vesicular glutamate transporter 3 in baboon retinas. Vis Neurosci. 2015; 32:E006. [PubMed: 26241195]

McMahon MJ, Packer OS, Dacey DM. The classical receptive field surround of primate parasol ganglion cells is mediated primarily by a non-GABAergic pathway. J Neurosci. 2004; 24:3736–3745. [PubMed: 15084653]

Merigan WH, Katz LM, Maunsell JH. The effects of parvocellular lateral geniculate lesions on the acuity and contrast sensitivity of macaque monkeys. J Neurosci. 1991; 11:994–1001. [PubMed: 2010820]

Morgan JL, Schubert T, Wong RO. Developmental patterning of glutamatergic synapses onto retinal ganglion cells. Neural Dev. 2008; 3:8. [PubMed: 18366789]

Münch TA, da Silveira RA, Siegert S, Viney TJ, Awatramani GB, Roska B. Approach sensitivity in the retina processed by a multifunctional neural circuit. Nat Neurosci. 2009; 12:1308–1316. [PubMed: 19734895]

Percival KA, Koizumi A, Masri RA, Buzás P, Martin PR, Grünert U. Identification of a pathway from the retina to koniocellular layer K1 in the lateral geniculate nucleus of marmoset. J Neurosci. 2014; 34:3821–3825. [PubMed: 24623761]

Polyak, SP. The Retina. Illinois: The University of Chicago Press; 1941.

Polyak, SP. The Vertebrate Visual System. Illinois: The University of Chicago Press; 1957.

Protti DA, Di Marco S, Huang JY, Vonhoff CR, Nguyen V, Solomon SG. Inner retinal inhibition shapes the receptive field of retinal ganglion cells in primate. J Physiol. 2014; 592:49–65. [PubMed: 24042496]

Purpura K, Kaplan E, Shapley RM. Background light and the contrast gain of primate P and M retinal ganglion cells. Proc Natl Acad Sci USA. 1988; 85:4534–4537. [PubMed: 3380804]

Rovamo J, Raninen A. Critical flicker frequency as a function of stimulus area and luminance at various eccentricities in human cone vision: a revision of Granit-Harper and Ferry-Porter laws. Vision Res. 1988; 28:785–790. [PubMed: 3227655]

Sampath AP, Rieke F. Selective transmission of single photon responses by saturation at the rod-to-rod bipolar synapse. Neuron. 2004; 41:431–443. [PubMed: 14766181]

Schiller PH, Logothetis NK, Charles ER. Functions of the colour-opponent and broad-band channels of the visual system. Nature. 1990; 343:68–70. [PubMed: 2296292]

Schnapf JL, Nunn BJ, Meister M, Baylor DA. Visual transduction in cones of the monkey Macaca fascicularis. J Physiol. 1990; 427:681–713. [PubMed: 2100987]

Schneeweis DM, Schnapf JL. Photovoltage of rods and cones in the macaque retina. Science. 1995; 268:1053–1056. [PubMed: 7754386]

Seiple W, Holopigian K. Outer-retina locus of increased flicker sensitivity of the peripheral retina. J Opt Soc Am A Opt Image Sci Vis. 1996; 13:658–666. [PubMed: 8627423]

Sivyer B, Taylor WR, Vaney DI. Uniformity detector retinal ganglion cells fire complex spikes and receive only light-evoked inhibition. Proc Natl Acad Sci USA. 2010; 107:5628–5633. [PubMed: 20212117]

Solomon SG, Martin PR, White AJ, Rüttiger L, Lee BB. Modulation sensitivity of ganglion cells in peripheral retina of macaque. Vision Res. 2002; 42:2893–2898. [PubMed: 12450500]

Tyler CW. Analysis of visual modulation sensitivity. II. Peripheral retina and the role of photoreceptor dimensions. J Opt Soc Am A. 1985; 2:393–398. [PubMed: 3981280]

Venkataramani S, Taylor WR. Orientation selectivity in rabbit retinal ganglion cells is mediated by presynaptic inhibition. J Neurosci. 2010; 30:15664–15676. [PubMed: 21084622]

Venkataramani S, Van Wyk M, Buldyrev I, Sivyer B, Vaney DI, Taylor WR. Distinct roles for inhibition in spatial and temporal tuning of local edge detectors in the rabbit retina. PLoS ONE. 2014; 9:e88560. [PubMed: 24586343]

Verweij J, Hornstein EP, Schnapf JL. Surround antagonism in macaque cone photoreceptors. J Neurosci. 2003; 23:10249–10257. [PubMed: 14614083]

Wässle H, Grünert U, Röhrenbeck J, Boycott BB. Cortical magnification factor and the ganglion cell density of the primate retina. Nature. 1989; 341:643–646. [PubMed: 2797190]

Wässle H, Grünert U, Chun MH, Boycott BB. The rod pathway of the macaque monkey retina: identification of AII-amacrine cells with antibodies against calretinin. J Comp Neurol. 1995; 361:537–551. [PubMed: 8550898]

Waugh SJ, Hess RF. Suprathreshold temporal-frequency discrimination in the fovea and the periphery. J Opt Soc Am A Opt Image Sci Vis. 1994; 11:1199–1212. [PubMed: 8189283]

Wei W, Hamby AM, Zhou K, Feller MB. Development of asymmetric inhibition underlying direction selectivity in the retina. Nature. 2011; 469:402–406. [PubMed: 21131947]

Wikler KC, Williams RW, Rakic P. Photoreceptor mosaic: number and distribution of rods and cones in the rhesus monkey retina. J Comp Neurol. 1990; 297:499–508. [PubMed: 2384610]

Wu SM. Feedback connections and operation of the outer plexiform layer of the retina. Curr Opin Neurobiol. 1992; 2:462–468. [PubMed: 1525544]

Yin L, Masella B, Dalkara D, Zhang J, Flannery JG, Schaffer DV, Williams DR, Merigan WH. Imaging light responses of foveal ganglion cells in the living macaque eye. J Neurosci. 2014; 34:6596–6605. [PubMed: 24806684]

Yonehara K, Balint K, Noda M, Nagel G, Bamberg E, Roska B. Spatially asymmetric reorganization of inhibition establishes a motion-sensitive circuit. Nature. 2011; 469:407–410. [PubMed: 21170022]

Highlights

- Cone photoreceptor kinetics dictates temporal sensitivity of our visual perception
- Foveal midget ganglion cells (MGCs) receive little or no synaptic inhibition
- Foveal but not peripheral MGCs express few inhibitory postsynaptic receptors
- Postsynaptic inhibition controls gain but not kinetics of MGC responses

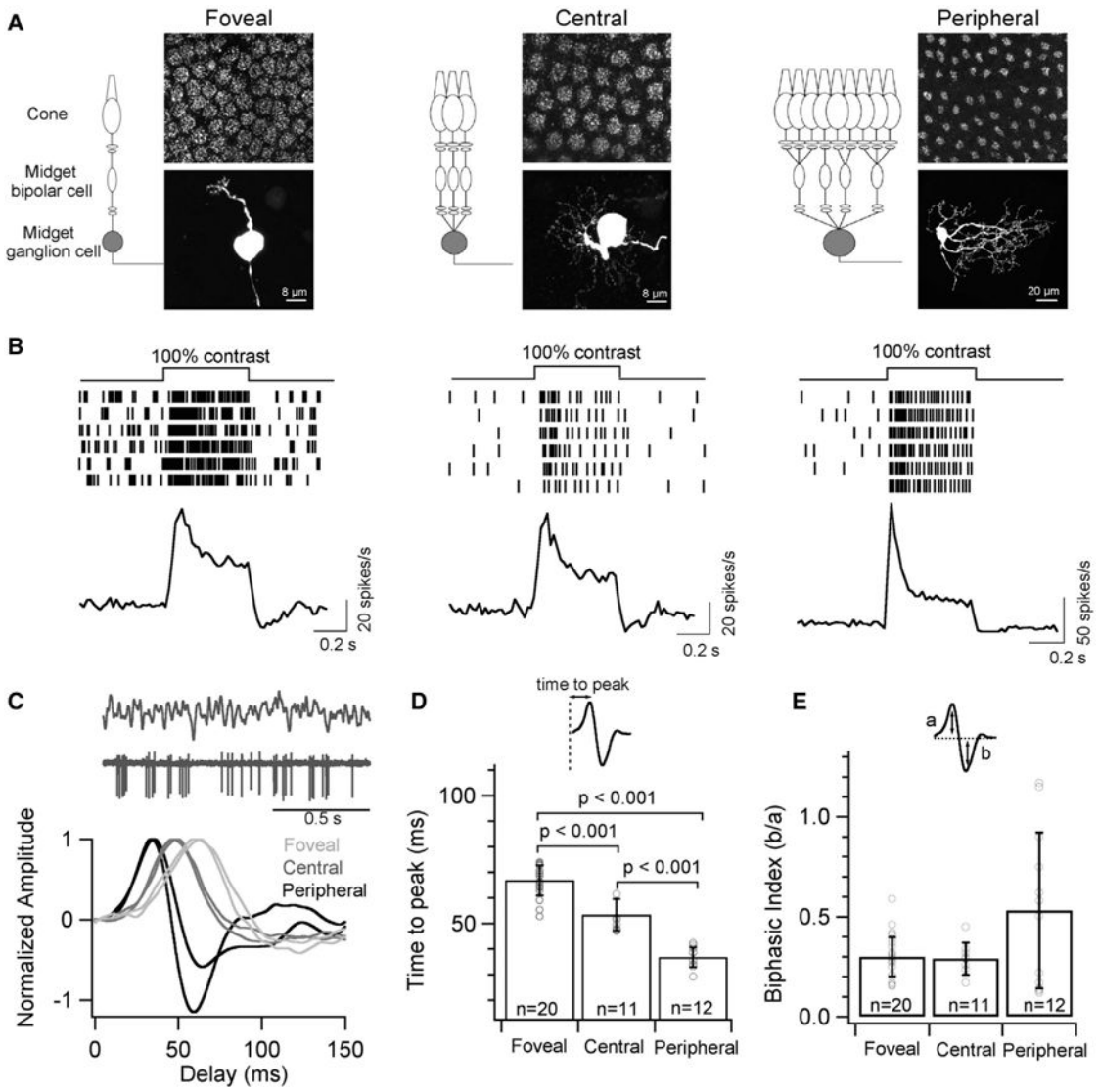

Figure 1. Midget Ganglion Cells Show Slower Response Kinetics in the Fovea than in the Periphery

(A) Schematic depicting the convergence of the midget circuit in primate retina at three different eccentricities. MGCs were classified as foveal (<1 mm), central (2–4 mm), and peripheral (>6 mm) based on their distance from the foveal pit. Top panel shows a composite fluorescence micrograph of AMPA receptor subunit, GluA3, at the outer plexiform layer indicating the cone density and the bottom panel is the corresponding image of a neurobiotin-filled MGC at each eccentricity.

(B) Spike trains from six trials of an exemplar MGC and the average peri-stimulus time histogram (binwidth of 20ms) across several MGCs at each retinal eccentricity in response to a full-field 100% contrast light step. Note the transient spike response from peripheral MGCs.

(C) Temporal receptive field probed with a full-field Gaussian white noise stimuli. A short excerpt of the stimulus and spike response (top) with exemplar time-reversed spike-triggered average (STA) of individual MGCs at each retinal eccentricity (bottom).

(D) Quantification of the time to peak i.e., latency of the peaks in STAs yields a mean of 67 ± 6 ms for foveal MGCs, 53 ± 6 ms for central MGCs and 37 ± 4 ms for peripheral MGCs. The latency of the STAs is significantly longer for foveal MGCs than central or peripheral MGCs.

(E) Quantification of the biphasic index of STAs i.e., the ratio of the peak amplitudes from the baseline yields a mean value of 0.33 ± 0.15, 0.30 ± 0.06 and 0.51 ± 0.35 for MGCs in foveal, central and peripheral retina, respectively. In all figures, error bars indicate s.d. and ‘n’ refers to the number of cells analyzed.

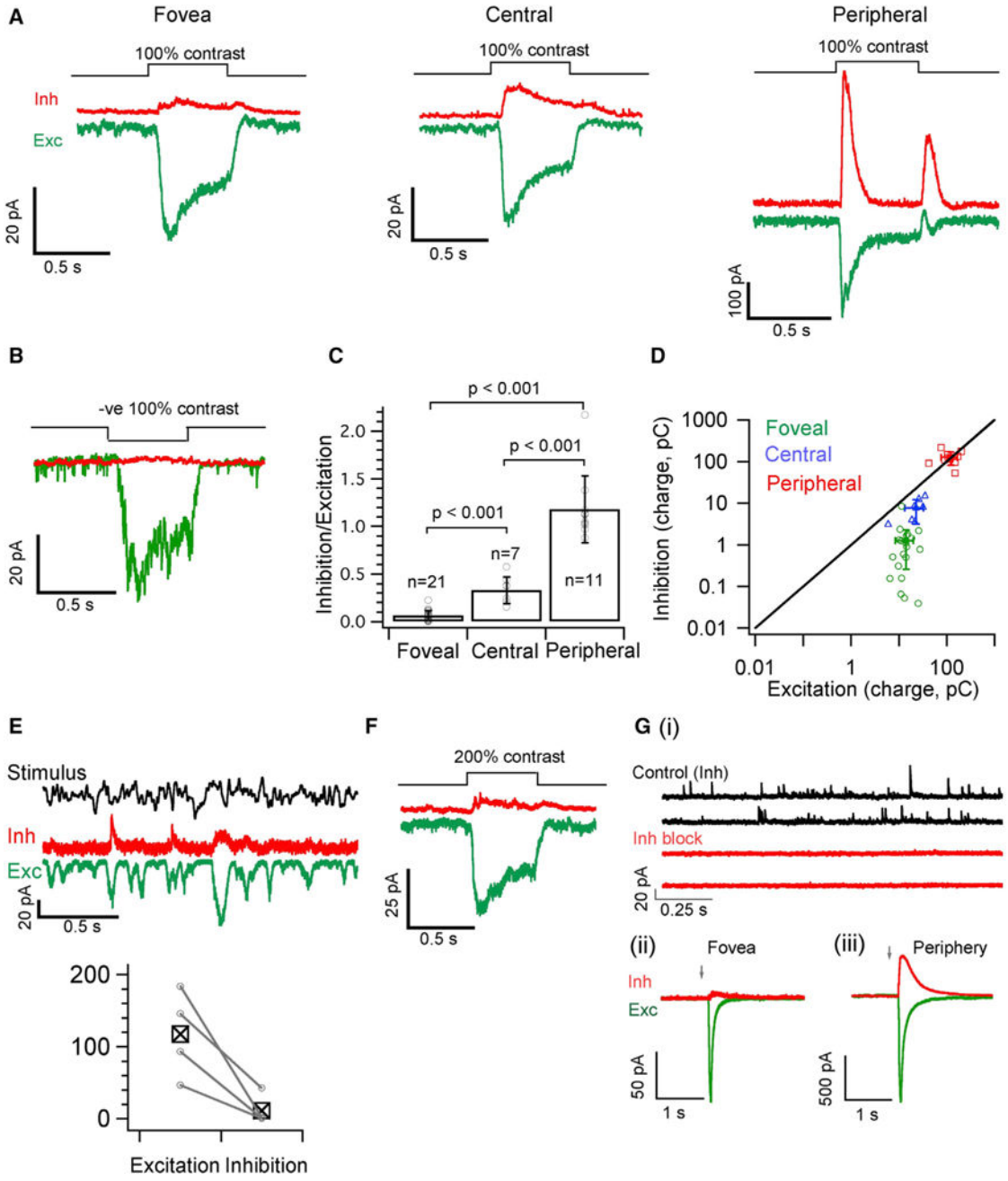

Figure 2. Foveal Midget Ganglion Cells Receive Little or No Light-Evoked Inhibition

(A) Average excitatory (Exc, in green) and inhibitory (Inh, in red) synaptic currents produced by a 100% contrast light step (background light intensity of 4,000 R*/cone/sec) from voltage-clamped MGCs in foveal, central and peripheral retina.

(B) Mean excitatory (green) and inhibitory (red) synaptic current in response to a negative 100% contrast step measured from a voltage-clamped foveal OFF MGC.

(C) Ratio of the inhibitory to excitatory charge transfer analyzed from individual MGC response to a contrast light step as shown in A for each of the retinal locations. The mean I/E

ratio is 0.06 ± 0.05, 0.33 ± 0.14 and 1.18 ± 0.35 for foveal, central and peripheral MGCs respectively.

(D) 2D plot of absolute excitatory versus inhibitory charge transfer across eccentricity (raw values used to calculate I/E ratio in Figure 2C). The average value for peripheral MGCs lies on the unity line whereas foveal and central MGCs are below the unity line and skewed toward excitation.

(E) Exemplar average trace of inhibitory and excitatory synaptic currents of foveal ON MGCs in response to a time varying stimulus. Bottom panel shows a pairwise comparison of stimulus-driven variance in excitatory and inhibitory responses across 4 foveal ON MGCs.

(F) Mean excitatory (green) and inhibitory (red) synaptic current in response to a positive 200% contrast step measured from voltage-clamped foveal ON MGCs (n = 5).

(G) (i), Spontaneous inhibitory synaptic currents (Control Inh) are often observed in foveal MGCs and are blocked after bath application of GABA and Glycine receptor blockers (Inh block).

(G) (ii & iii), Simultaneous uncaging of Glutamate and GABA on the dendrites of foveal and Peripheral MGCs. Average traces of currents evoked by Glutamate (green; MNI-Glutamate) and GABA (red; Rubi-GABA) uncaging from foveal and peripheral MGCs (n = 3) voltage clamped at the inhibitory or excitatory reversal potential. Arrow indicates time of uncaging. The ratio of inhibition to excitation (charge transfer) yields a mean value of 0.1 ± 0.07 and 0.84 ± 0.5 for foveal and peripheral MGCs respectively. See also Figure S5.

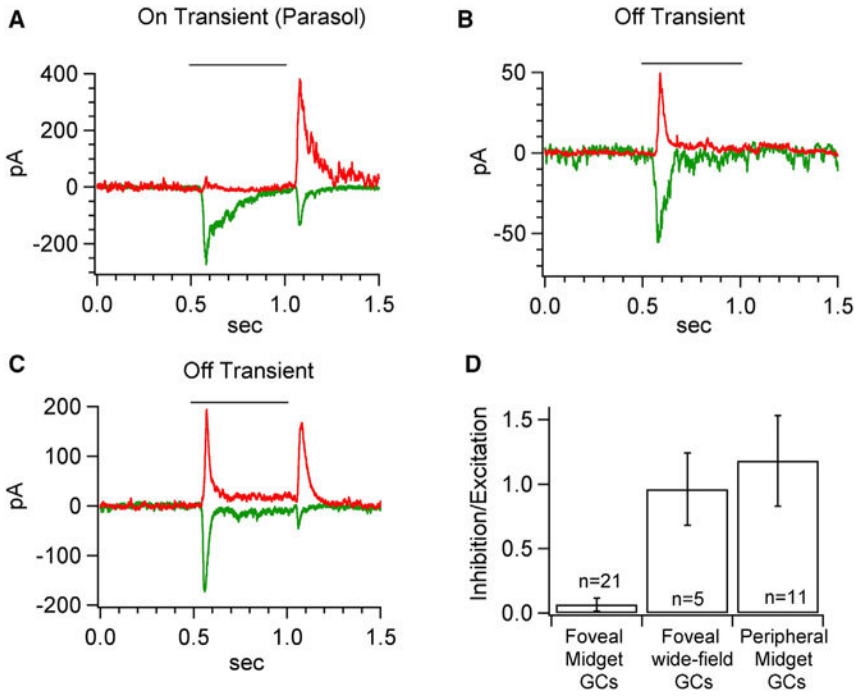

Figure 3. Excitatory and Inhibitory Responses of Foveal Wide-Field Ganglion Cells

(A–C) Exemplar mean excitatory (green) and inhibitory (red) synaptic current in response to a 100% contrast step measured from voltage-clamped foveal wide-field ganglion cells.

(D) Comparison of the ratio of inhibitory to excitatory charge transfer to a 100% contrast light step as shown in Figures 2A and C. The mean I/E ratio is 0.06 ± 0.05, 1.0 ± 0.3 and 1.2 ± 0.4 for foveal MGCs (data from Figure 2), foveal wide-field ganglion cells and peripheral MGCs (data from Figure 2) respectively.

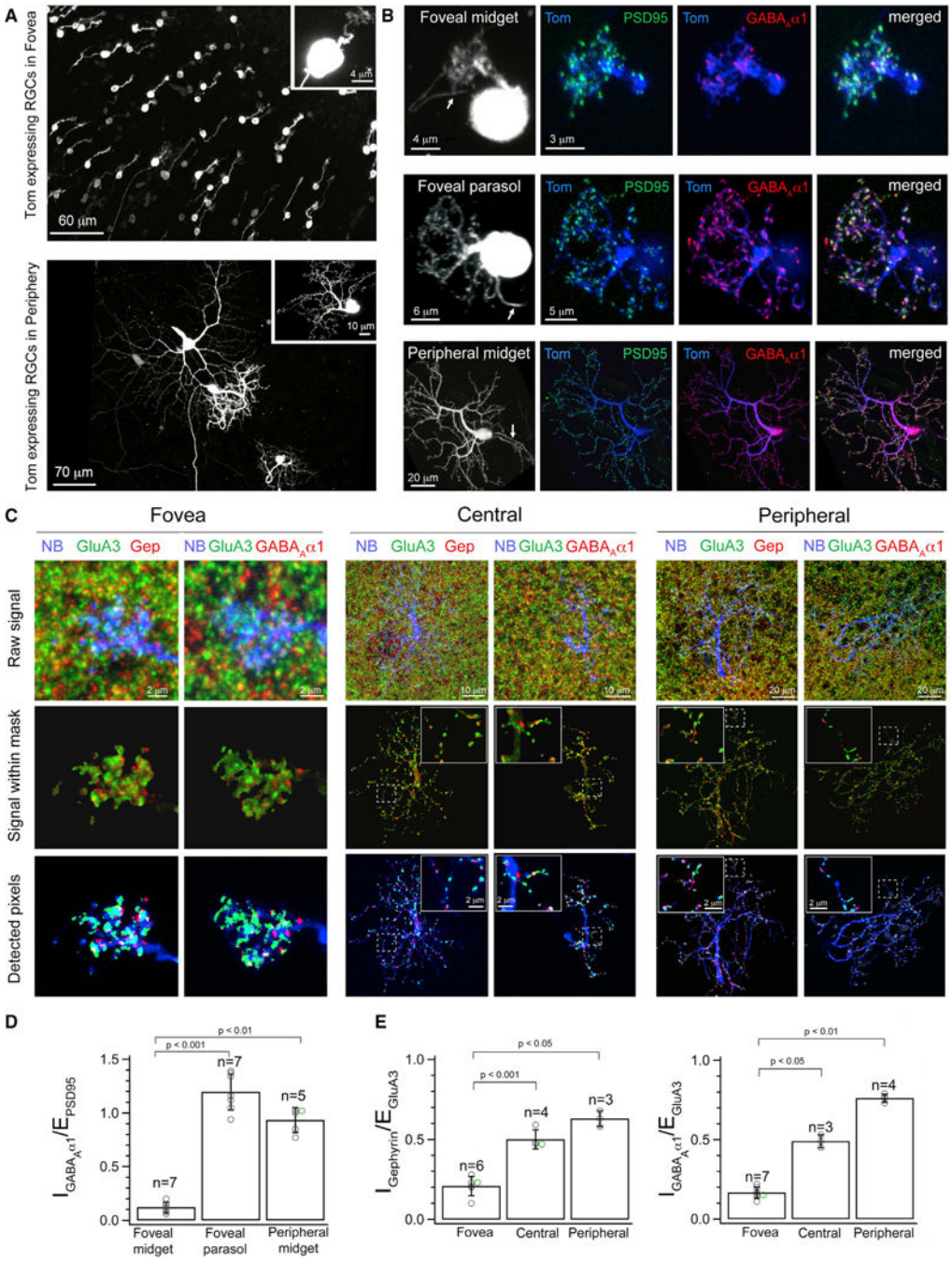

Figure 4. Foveal Midget Ganglion Cells Express Low Levels of Inhibitory Postsynaptic Receptors Relative to Excitatory Postsynaptic Receptors

(A), Whole-mount view of retinal ganglion cells (RGCs) biolistically labeled by expression of tdTomato (Tom) in foveal (top) and peripheral (bottom) macaque retina. Inset shows a single MGC at each eccentricity.

(B) Maximum intensity projection of a co-transfected MGC and parasol cell in the macaque fovea and a MGC in peripheral retina. Arrows point to the axon. PSD95-CFP (green) and $GABA_A\alpha1$-YFP (red) expression in tdTomato (Tom, blue) labeled cells.

(C) Maximum intensity projections showing neurobiotin-filled (NB, blue) dendrites of MGCs colabeled with GluA3 (green) and gephyrin (Gep, red) or with GluA3 and $GABA_A\alpha1$-YFP (red) at each of the three different retinal eccentricities (foveal, central, peripheral). Top panel shows the combined raw immunolabeling signal (see Figure S2 for individual labeling panels). Middle panel shows the receptor signal within the masked MGC dendritic process. Bottom panel shows the receptor pixels above a threshold that eliminates background fluorescence associated with the immunolabeling (see STAR Methods and Figure S3). Insets for central and peripheral MGCs show raw and detected GluA3 and gephryin signal or GluA3 and $GABA_A\alpha1$-YFP signal along a small dendritic stretch.
(D) Quantification of the % volume occupancy of $GABA_A\alpha1$-YFP signal relative to PSD95-CFP signal within tdTomato filled dendrites in the fovea revealed a much higher $I_{GABAA}/E_{PSD\text{-}95}$ ratio in parasol cells (mean = 1.22 ± 0.25) relative to MGCs (mean of 0.14 ± 0.05). MGCs also revealed a low-fovea to high-periphery $I_{GABAA}/E_{PSD\text{-}95}$ ratio across eccentricity (periphery, mean of 0.88 ± 0.13). The overlapping data points have been shifted and color-coded for better clarity.
(E) Quantification of the $I_{Gephyrin}/E_{GluA3}$ ratio by estimation of the % volume (dendrite) occupancy of gephyrin signal as compared to the % occupancy of the GluA3 signal. The $I_{Gephyrin}/E_{GluA3}$ ratio for neurobiotin filled MGCs was significantly lower in foveal (mean of 0.21 ± 0.06) compared to central (mean of 0.50 ± 0.06) and peripheral (mean of 0.60 ± 0.05) retina. Similar results were obtained upon quantification of the I_{GABAA}/E_{GluA3} ratio for neurobiotin filled MGCs (foveal, mean of 0.17 ± 0.04; central, mean of 0.49 ± 0.04; peripheral, mean of 0.76 ± 0.03). The overlapping data points have been shifted and color-coded for better clarity. See also Figures S1, S2, S3, S4, and S6.

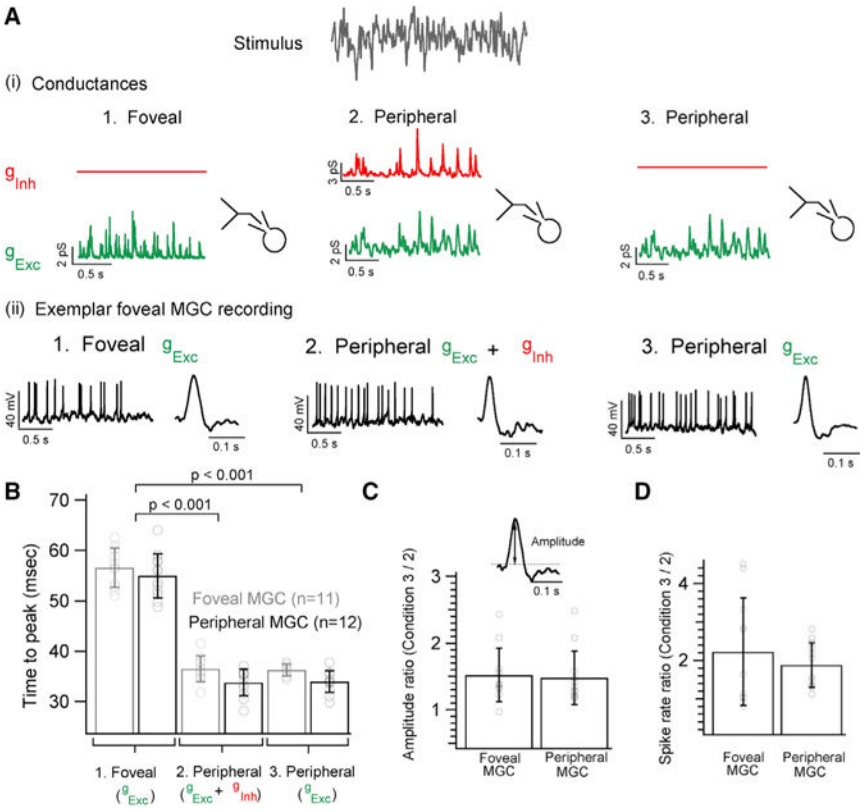

Figure 5. Inhibitory Synaptic Input Affects Gain but Not Kinetics of Peripheral Midget Ganglion Cell Outputs

(A) Dynamic clamp experiment illustrating the three sets of conductances injected into foveal or peripheral MGCs. (1) Synaptic conductances were measured in response to white noise stimuli as in Figure 1C: 1. Foveal g_{Exc} 2. Peripheral g_{Exc} + g_{Inh} and 3. Peripheral g_{Exc} (2) Exemplar current-clamp recording from a foveal MGC where each of the three sets of conductances evokes corresponding spike responses. Exemplar STA from a foveal MGC for each of the three injected conductance sets.

(B) Bar graph comparing the time to peak of the STAs for each of the three conductance sets for foveal and peripheral MGCs. MGCs show faster kinetics with shorter time to peak when injected with peripheral synaptic conductances at the fovea (mean of 36 ± 3 ms for g_{Exc} + g_{Inh} and 36 ± 1 ms for g_{Exc}) and in the periphery (mean of 34 ± 3 ms for g_{Exc} + g_{Inh} and 34 ± 2 ms for g_{Exc}). However, when MGCs are injected with foveal conductances their response kinetics gets appreciably slower (mean of 57 ± 4 ms for foveal MGCs and mean of 55 ± 4 ms for peripheral MGCs).

(C) Ratio of the STA amplitude measured from MGCs without peripheral inhibitory conductances (set 3 in A) to those measured with peripheral inhibitory conductances (set 2 in A) yields a mean value of 1.5 ± 0.4 for both foveal and peripheral MGCs.

(D) The ratio of the mean spike rate yields a mean value of 2.2 ± 1.4 and 1.9 ± 0.5 for foveal and peripheral MGCs, respectively.

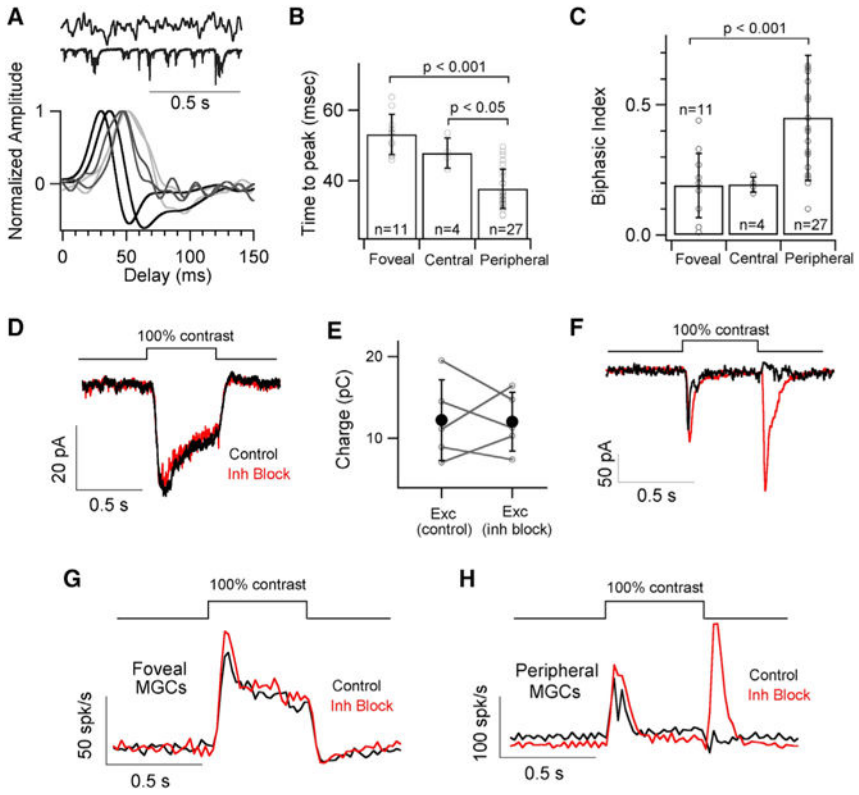

Figure 6. Excitatory Inputs on MGCs Exhibit a Gradient of Kinetics across Retinal Locations

(A) Short excerpt of the white noise stimulus and excitatory synaptic response (top) with exemplar time-reversed linear filters for excitatory synaptic currents measured in response to white noise stimuli.

(B) Quantification of the time to peak for the linear filters yields a mean of 53 ± 6 ms, 48 ± 4 ms and 38 ± 6 ms for foveal, central and peripheral MGCs, respectively.

(C) Bar graph comparing the biphasic indices of linear filters from MGCs in foveal, central and peripheral retina. The mean biphasic indices are 0.19 ± 0.12, 0.19 ± 0.03 and 0.45 ± 0.24 for foveal, central and peripheral MGCs.

(D) Average excitatory synaptic currents in response to a 100% contrast light step from foveal MGCs before and after bath application of a cocktail of GABA and Glycine receptor blockers (TPMPA, GABAzine and Strychnine).

(E) A pairwise comparison of charge transfer of the excitatory response from individual MGCs (n = 5) before and after drug application (mean $Exc_{control}$ = 12.22 ± 4.92 pC and mean $Exc_{Inh\ block}$ = 12.02 ± 3.57 pC) shows no significant difference ($p > 0.05$).

(F) Mean excitatory synaptic current in response to a 100% contrast step before (black trace) and after (red trace) bath application of GABA and Glycine receptor blockers (GABAzine, TPMPA and Strychnine) reveals an OFF response (i.e., response at the light offset) suggesting a key role of presynaptic inhibition in shaping peripheral MGC input.

(G and H) Average peri-stimulus time histogram (binwidth of 20ms) across foveal and peripheral MGCs in response to a full-field 100% contrast light step before (black trace) and after (red trace) bath application of inhibitory GABA and Glycine receptor blockers (GABAzine, TPMPA and Strychnine).

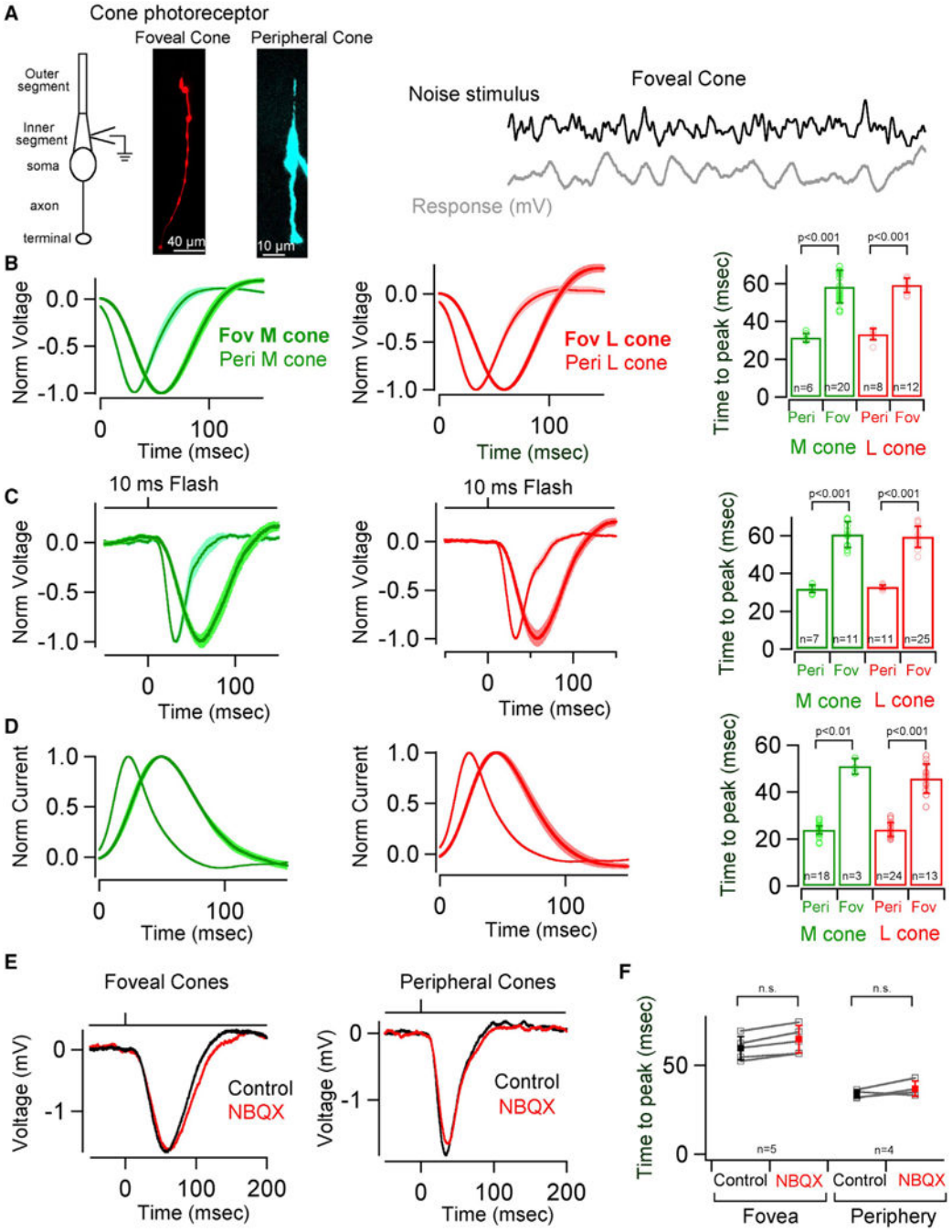

Figure 7. Cone Signals Are Slower in the Fovea than Periphery

(A) Schematic illustrating the morphology of a cone photoreceptor. Whole cell recordings were performed at the inner segment as depicted in the schematic. A cell-fill image of a foveal (Fov) and peripheral (Peri) cone. Please note the dramatic difference in cone morphology, particularly the long axon of the foveal cone. A short excerpt of a foveal cone voltage response to a time varying stimulus. Cone voltage responses (B, C and E) are depicted with an opposite polarity compared to current responses (D).

(B) Average time-reversed linear filters for foveal and peripheral M and L cone voltage responses. Shaded regions represent SEM. Quantification of the time to peak for the linear filters yields a mean of 31.45 ± 2 ms and 58.37 ± 9 ms for peripheral and foveal M cones, respectively. The mean time to peak for peripheral and foveal L cones was 33.2 ± 3 ms and 59.3 ± 4 ms, respectively. Error bars represent s.d.

(C) Average voltage responses of foveal and peripheral M and L cones to a 300% contrast light flash. Shaded regions represent SEM. Quantification of the time to peak for the responses yields a mean of 31.85 ± 2 ms and 60.68 ± 7 ms for peripheral and foveal M cones, respectively. The mean time to peak for peripheral and foveal L cones was 32.8 ± 1 ms and 59.44 ± 6 ms, respectively. Error bars represent s.d.

(D) Average time-reversed linear filters for foveal and peripheral M and L cone currents. Shaded regions represent SEM. Quantification of the time to peak for the linear filters yields a mean of 23.9 ± 2 ms and 51.03 ± 3 ms for peripheral and foveal M cones, respectively. The mean time to peak for peripheral and foveal L cones was 23.95 ± 3 ms and 45.76 ± 6 ms, respectively. Error bars represent s.d.

(E) Average voltage responses of foveal and peripheral cone photoreceptors to 300% contrast (10ms flash) under control conditions (black) and with AMPA receptors blocked (red) to eliminate cone transmission to horizontal cells (10 μM NBQX).

(F) Quantification of the time to peak of the voltage responses to 300% contrast (10ms flash) yields a mean of 59.72 ± 7 ms and 64.8 ± 8 ms for foveal cones before and after application of NBQX. The mean time to peak for peripheral cones before and after NBQX application was 33.28 ± 2 ms and 36.95 ± 4 ms, respectively. Error bars represent s.d. See also Figure S7.